# Analysis of the structural and electronic properties of $(fluoranthene)_2PF_6$ and characterization of its (011) surface by scanning tunneling microscopy

K.S. Lee [a,1], D.-K. Seo [a], J. Ren [a], M.-H. Whangbo [a], S.N. Magonov [b], G. Bar [c], W. Brütting [d]

[a] *Department of Chemistry, North Carolina State University, Raleigh, NC 27695-8204, USA*

[b] *Digital Instruments, Inc., 520 E. Montecito Street, Santa Barbara, CA 93103, USA*

[c] *Materials Research Center, Albert-Ludwigs University, Stefan-Meier-Strasse 21, D-79104 Freiburg, Germany*

[d] *Physikalisches Institut und Bayreuther Institut für Makromolekülforschung, Universität Bayreuth, D-95440 Bayreuth, Germany*

**Abstract**

The phase transitions of the conducting salts $(FA)_2X$ (FA = fluoranthene; X = $PF_6$, $AsF_6$) at 200 and 180 K were probed by analyzing the short intermolecular contacts of their crystal structures and calculating their electronic band structures. The scanning tunneling microscopy (STM) images of $(FA)_2PF_6$ were interpreted by calculating the partial electron density plots for its (011) surface. Our study indicates that the 200 K phase transition leads to a more compact crystal packing in which all F atoms of a $PF_6^-$ anion make short F···H contacts with the surrounding FA molecules. The 180 K phase transition originates from the charge density wave (CDW) instability of each FA stack. It is most likely that the dimerization expected from the CDW instability involves rotations of FA dimers around the stacking axis, and that the occurrence of domain structures in each FA stack prevents the observation of a dimerized structure by single-crystal X-ray diffraction. The STM images of $(FA)_2PF_6$ indicate that a few FA molecules under the STM tip apex undergo a reversible, rotational rearrangement.

*Keywords:* Structural properties; Electronic properties; Fluoranthene; Microscopy; Surfaces

## 1. Introduction

Fluoranthene (FA, **1**) forms conducting salts $(FA)_2X$

**1**

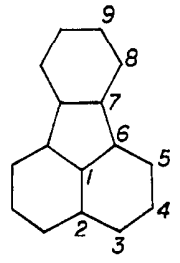


with the anions $X^- = PF_6^-$ and $AsF_6^-$, the structures and physical properties of which have been the subject of numerous studies [1–22]. In these salts, stacks of FA molecules running parallel to the *a*-direction are separated by the anions (Fig. 1) [3]. In each stack the FA molecules are slightly dimerized, and adjacent FA molecules have a 180°-rotation arrangement (**2**), so that each stack has two FA molecules per repeat unit (**3**). With the formal oxidation state $(FA)_2^+$, the highest occupied band of each FA stack is half-filled since there are two FA molecules per repeat unit (see Section 3). The structural and physical properties of the $(FA)_2X$ salts raise several important questions.

**2**

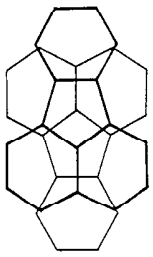

**3**

[1] Permanent address: Department of Chemistry, Catholic University of Korea, Puchon 422-743, South Korea.

$(FA)_2X$ undergoes two phase transitions as the temperature is lowered [3,4,6,7,14,16,17]. The first phase transition, which occurs at 200 K, is characterized by the rotation of each FA stack around the stacking axis. In terms of schematic projection views along the *a*-direction, the arrangements of the FA stacks above and below 200 K are given by **4a** and **4b**, respectively, where the rectangles represent the FA

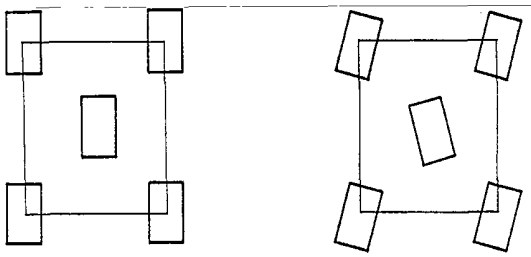

**4a** **4b**

stacks [3]. So far, the reason for this structural phase transition has not been explained. The second phase transition, which occurs at 180 K, is driven by the CDW instability associated with the half-filled band, because diffuse scattering corresponding to a CDW of wave vector $0.5a^*$ was observed [17]. This transition is expected to lower the symmetry of the crystal and double the repeat distance along the *a*-direction, but the *a*-axis doubling was not detected by single-crystal X-ray diffraction of $(FA)_2X$ determined at temperatures below 180 K [3,8]. In general, the cations and anions of organic conducting salts are held together with short intermolecular contacts [23,24]. In $(FA)_2X$ each FA stack is surrounded by the anions, and each column of the anions by the FA stacks (Fig. 1). This symmetry is broken on the surface of a crystal sample. It is important to examine whether

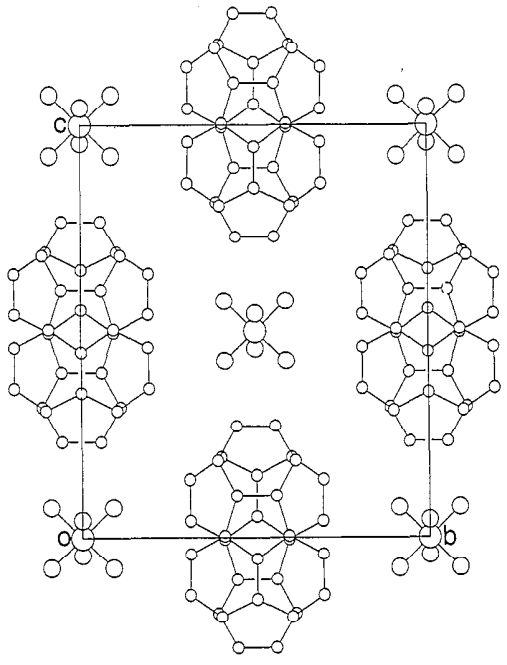


Fig. 1. Schematic projection view (along the *a*-direction) of the crystal structure of $(FA)_2PF_6$ at room temperature. The large, medium and small circles represent the P, F and C atoms, respectively.

the surface of $(FA)_2X$ undergoes a relaxation and, if so, whether it can be accounted for from the viewpoint of the bulk crystal structure of $(FA)_2X$.

In the present work, we analyze the electronic and crystal structures of $(FA)_2X$ to probe the questions described above. The electronic structures of $(FA)_2X$ were calculated using the extended Hückel tight binding electronic band structure method [25]. The (011) surface of $(FA)_2PF_6$ was characterized on the basis of the scanning tunneling microscopy (STM) images reported earlier [26]. We interpret the observed STM images by calculating the partial electron density plots [27–29], $\rho(r_0,e_f)$, of the (010) and (011) surfaces.

## 2. Intermolecular contacts and 200 K structural phase transition

The single-crystal X-ray crystal structure of $(FA)_2PF_6$ determined at room temperature does not have high resolution, nor does that of $(FA)_2AsF_6$ determined at 120 K [3]. The F positions of the $PF_6^-$ anions possess large standard deviations and large thermal ellipsoids. In addition, several C–H bonds of FA are bent out of the $\pi$-plane and have lengths significantly longer than 1.08 Å. To check the relevance of the latter findings, we performed full geometry optimizations of FA and its cation $FA^+$ on the basis of AM1 SCF-MO calculations using the MOPAC program [30]. These calculations show all C–H bonds of FA and $FA^+$ to be in the $\pi$-plane and have lengths very close to 1.08 Å. Thus, in our calculations of the short intermolecular contacts between the FA molecules and $PF_6^-$ anions in $(FA)_2PF_6$ (see below) as well as the $\rho(r_0,e_f)$ plots, we replaced the C–H bonds of FA with C–H = 1.08 Å along the C–H bond directions found in our AM1 SCF-MO calculations of FA.

Fig. 2(a)–(b) shows two perspective views of the short intermolecular contacts associated with one $PF_6^-$ anion in $(FA)_2PF_6$. Of the six F atoms of $PF_6^-$, only four make short H···F contacts with the C–H bonds of the surrounding FA molecules (2.32 Å along the *c*-direction and 2.46 Å along the *b*-direction). These H···F distances are shorter than the van der Waals distance (i.e., 2.70 Å) [31] but longer than the C–H···F hydrogen bond distance (about 2.20 Å) [32]. The remaining two F atoms of a $PF_6^-$ anion, arranged *trans* to each other, do not make short contacts with the surrounding FA molecules. In addition, the H···H contacts (2.41 and 2.50 Å) between the FA molecules surrounding a $PF_6^-$ anion are not shorter than the van der Waals distance (i.e., 2.40 Å). All these can be a source of structural instability, because it means the presence of unused space in crystal packing. The primary role of the 200 K phase transition would be to let the crystal have a more compact packing in which all F atoms of $PF_6^-$ engage in short C–H···F contacts. The X-ray crystal structure of $(FA)_2AsF_6$ determined at 120 K [3] indicates that this is indeed the case.

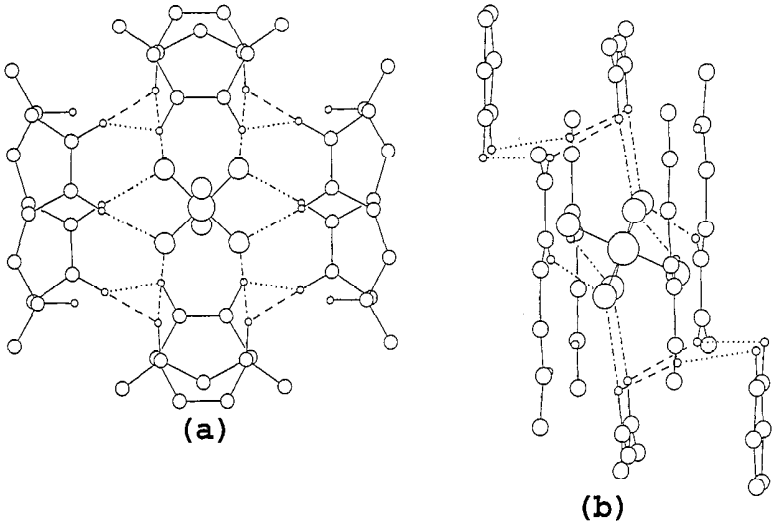


Fig. 2. Schematic projection views of the short intermolecular contacts around a $PF_6^-$ anion in the crystal structure of $(FA)_2PF_6$ at room temperature: (a) approximately along the *a*-direction and (b) approximately along the *b*-direction. The P and H atoms are represented by the largest and smallest circles, respectively, and the F and C atoms by the second largest and second smallest circles, respectively. The H···H contact distances are 2.50 Å (· · ·) and 2.41 Å (– – –). The F···H contact distances are 2.31 Å (– · –) and 2.46 Å (– ··· –).

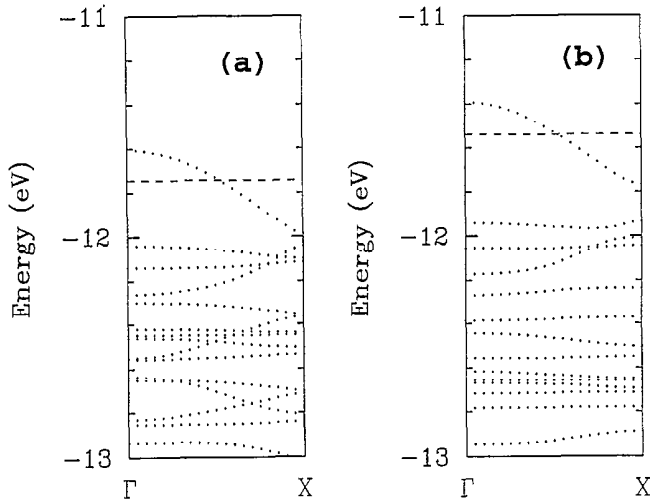


Fig. 3. Dispersion relations of the electronic band structures calculated for isolated FA stacks in the crystal structures of (a) $(FA)_2PF_6$ at room temperature and (b) $(FA)_2AsF_6$ at 120 K. The Fermi level is represented by a dashed line.

## 3. Electronic structure and 180 K phase transition

The HOMO of FA calculated by AM1 SCF-MO calculations is schematically shown in the projection view **5**. As

**5**

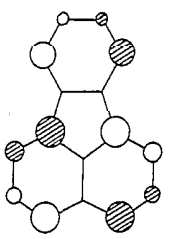

already found in other studies [10,13,19], large coefficients in the HOMO are found for the C(3), C(6) and C(8) atoms. (For the numbering of the carbon atoms of FA, see **1**.) The coefficients of the C3, C4, C5, C6, C8 and C9 are 0.36, 0.22, −0.26, −0.37, 0.30 and 0.16, respectively. In the 180°-rotation arrangement (**2**), the C3, C6 and C8 atoms of one FA molecule are positioned above the C8, C6 and C3 atoms of the other FA molecule, respectively. This leads to a strong HOMO–HOMO overlap between adjacent FA molecules.

Fig. 3(a) shows the dispersion relations of the energy bands calculated for an isolated FA stack of $(FA)_2PF_6$ at room temperature, and Fig. 3(b) those calculated for an isolated FA stack of $(FA)_2AsF_6$ at 120 K. Since there are two FA molecules per unit cell, the band resulting from the HOMO of FA is folded. This band is split into two sub-bands due to the low symmetry of the crystal. The overall width of this band is about 0.66 eV, so that the hopping integral between FA molecules is about 0.16 eV.

In both Fig. 3(a) and (b), the highest occupied band (i.e., the upper sub-band) is half-filled. This is consistent with the

metallic character of $(FA)_2X$ above 200 K, but not with the semiconducting character of $(FA)_2X$ below 180 K [6,7,16]. The latter problem originates from the crystal structure of $(FA)_2AsF_6$ at 120 K; each FA stack has two FA molecules per repeat unit as in the case of the room temperature structure [3]. A distortion doubling the *a*-axis length is required to open a bandgap at the Fermi level of the half-filled band, because it is dispersive along the *a*-direction. However, this is not apparent from the crystal structures of $(FA)_2X$ determined below 180 K [3,8].

Each FA stack can be considered as made up of FA dimers because of the 180°-rotation arrangement between adjacent FA molecules. The intra- and inter-dimer distances in the FA stack differ only slightly (3.28 Å versus 3.33 Å in $(FA)_2PF_6$ at room temperature; 3.22 Å versus 3.28 Å in $(FA)_2AsF_6$ at 120 K). Thus, the FA molecules within each stack are closely packed, so that the dimerization of each FA stack leading to four FA molecules per unit cell would be difficult if this were to change the intra- and inter-dimer distances. Alternatively, dimerization of each FA stack can be achieved when adjacent FA dimers rotate around the stacking axis such that their rotational directions are opposite. Rotations of the FA dimers should induce those of the neighboring anions in contact with them such that each column of anions along the *a*-direction has two anions per repeat unit. This 'rotational' dimerization is most probable because the thermal ellipsoids of the atoms of the FA molecules and anions exhibit shapes consistent with such rotations [8]. The rotational rearrangement, which occurs to lower the electronic energy, will induce strain into the lattice. In principle, each FA molecule is free to rotate in two directions, and so is each FA pair. Therefore, it is probable that the extent of strain is reduced when domain structures are formed within each FA stack by introducing rotational kinks (i.e., domain walls). Examples of such kinks are schematically illustrated in **6**, where the arrows refer to the rotational directions of the FA molecules around the stacking axis, and the kinks are surrounded by rectangular boxes. The formation of domain structures is expected to prevent a long range order of the rotational dimerization within each FA stack and between FA stacks and, hence, the observation of a dimerized structure by single-crystal X-ray diffraction.

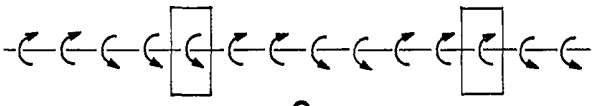

**6**

## 4. STM image and reversible local relaxation of the (011) surface

$(FA)_2PF_6$ was examined by STM earlier [26] under ambient conditions. Fig. 4(a)–(b) shows unfiltered and filtered STM images obtained for $(FA)_2PF_6$, respectively, and Fig. 4(c) a zoomed-in part of the image in Fig. 4(b). The surface unit cell of the image in Fig. 4(c) has the dimensions (i.e., 6.7 Å, 10 Å, 95°) that are consistent with the (011) surface rather than with the (010) surface of $(FA)_2PF_6$ [26]. In $(FA)_2PF_6$, layers of the $FA^{0.5+}$ cations alternate with layers of the $PF_6^-$ anions along the direction perpendicular to the (011) surface (Fig. 1). In principle, the (011) surface can be either the cation or the anion layer. However, the stacks of bright strips in the STM image show that the observed surface is the cation layer [26]. The most striking features of the STM images of $(FA)_2PF_6$ are that the FA molecules look more strongly paired than expected from the crystal structure, and that each FA molecule consists of two pieces of unequal lengths in many places.

The $\rho(r_0,e_f)$ plot calculated for the non-reconstructed cation layer of $(FA)_2PF_6$ on the (011) surface is shown in Fig. 5(a). For each FA dimer in a given FA stack, the electron densities are found around the C8 and C9 atoms in one FA and the C3 and C4 atoms in the other FA, i.e., the most protruding atoms on the non-reconstructed (011) surface. Thus, the length of a FA molecule seen from the electron density distribution of the $\rho(r_0,e_f)$ plot is much shorter than that deduced from a bright strip of the STM image. This discrepancy indicates that the structure of the cation layer

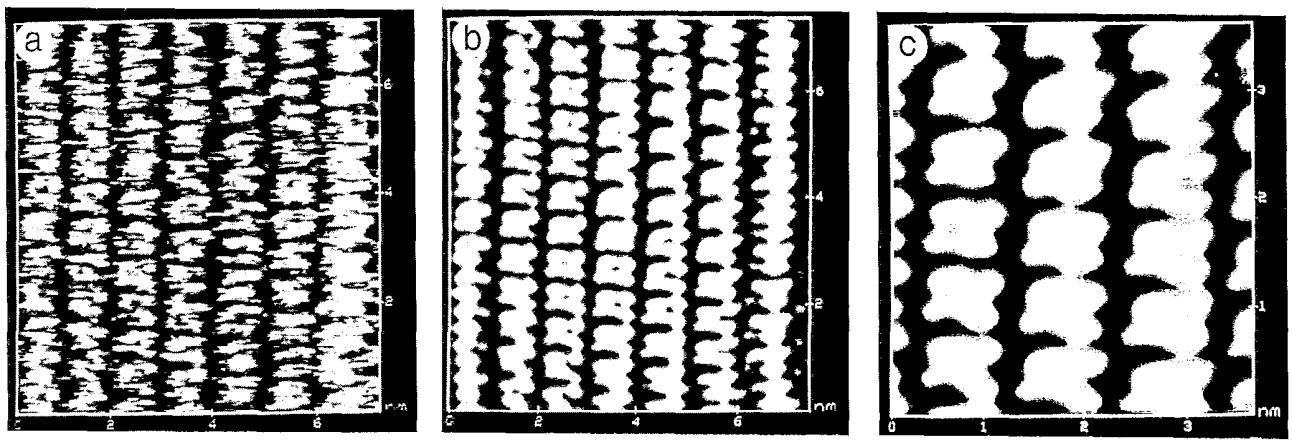


Fig. 4. STM images obtained for the (011) surface of $(FA)_2PF_6$: (a) unfiltered image ($V_{bias}$ = 423 mV, $I_{set}$ = 0.76 nA); (b) filtered image of (a); (c) zoomed-in part of (b). The contrast covers height variations in the 0.0–1.3 nm range in (a), in the 0.0–0.8 nm range in (b), and in the 0.0–1.0 nm range in (c).

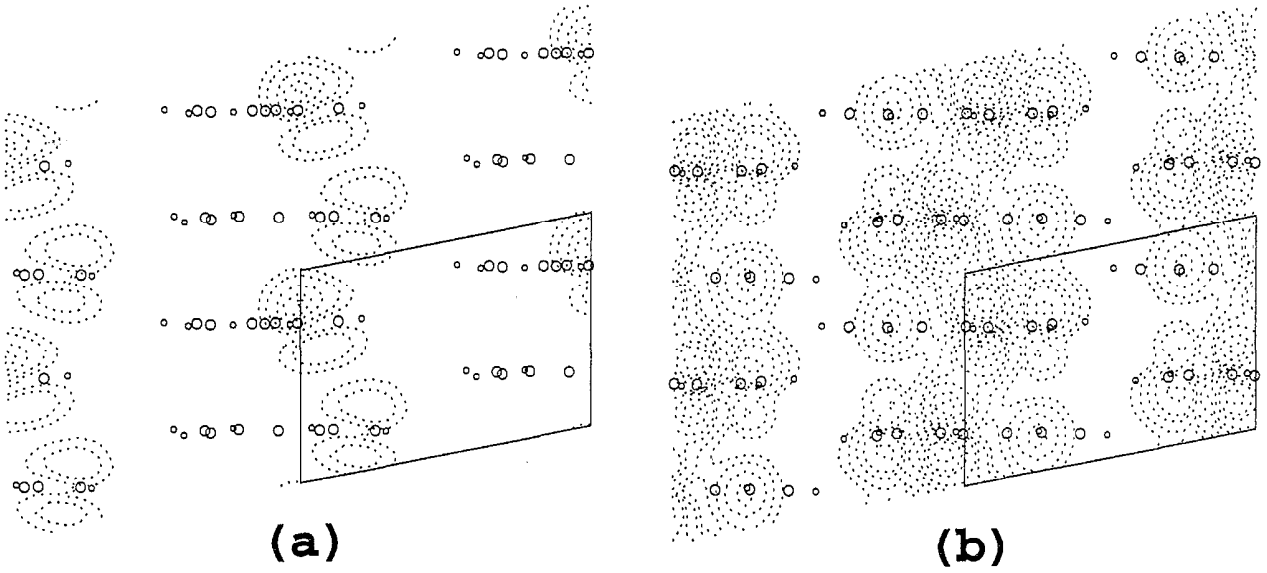


Fig. 5. $\rho(r_0,e_f)$ plots calculated for the cation layer on the (011) surface of $(FA)_2PF_6$: (a) non-reconstructed layer; the contour values used are 0.10, 0.08, 0.05, 0.02 and $0.008\times10^{-4}$ electrons/a.u.$^3$; (b) reconstructed layer for $\theta=41°$ and $\phi=\pm5°$. The contour values used are 0.10, 0.08, 0.05, 0.02 and $0.008\times10^{-4}$ electrons/a.u.$^3$. The C and H atoms of FA are represented by large and small circles, respectively. Each parallelogram represents one surface unit cell.

under the tip apex is different from that expected from the bulk crystal structure.

Given the molecular geometry of FA (**1**) and its stack structure, each FA molecule can appear longer in the $\rho(r_0,e_f)$ plot only if it is rotated around the stacking axis such that the plot has electron densities around the C4, C5 and C8 atoms (or around the C5, C8 and C9 atoms). It is convenient to describe such a rotational rearrangement in terms of two successive rotations ($\theta$ and $\phi$) around the stacking axis: (a) the rotation $\theta$ of each FA stack to make the C1–C2 bond axis of each FA parallel to the (011) surface (i.e., $\theta=41°$) and then (b) the rotation $\phi$ of each FA molecule to bring the C8 atom closer to the (011) surface. (The C8 and C4 atoms are equally close to the (011) surface when $\phi=\pm12°$.) To generate a $\rho(r_0,e_f)$ plot reproducing all essential features of the observed STM images, we calculate $\rho(r_0,e_f)$ plots of the cation layer as a function of $\theta$ and $\phi$. Fig. 5(b) shows the $\rho(r_0,e_f)$ plot for $\theta=41°$ and $\phi=\pm5°$. Several features of this plot are noteworthy: the electron density of C4 is comparable in magnitude to that of C8, the electron densities of C5 and C4 appear merged while the electron density of C8 is separated from that of C5, and the electron density within a FA dimer is higher than that between dimers. These features are entirely consistent with the observed STM images.

It is important to note that the structure of the cation layer employed for the calculation of the $\rho(r_0,e_f)$ plot in Fig. 5(b) is unreasonable, because some intermolecular H···H contacts are extremely short (e.g., about 1.5 Å). Therefore, one has to consider how this problem can be reconciled with the finding that the $\rho(r_0,e_f)$ plot and STM image are in excellent agreement. It should be recalled that the overall STM or atomic force microscopy (AFM) image refers to a collection of local images seen by the tip apex. Thus, a surface relaxation presented by an STM or AFM image may simply be a reversible local phenomenon, as found for a number of layered inorganic materials [29,33–37]. The STM image of $(FA)_2PF_6$ is explained if the rotational rearrangement discussed above (e.g., $\theta=41°$ and $\phi=\pm5°$) is a reversible local phenomenon: under the tip apex, only several FA molecules of one stack adopt the rotational rearrangement, and the adjacent FA molecules relax their positions to prevent the formation of unreasonably short intermolecular H···H contacts.

## 5. Concluding remarks

The crystal and electronic structures of $(FA)_2X$ ($X=PF_6$, $AsF_6$) were analyzed in some detail to help understand their two phase transitions. The structural phase transition at 200 K occurs most probably to have a more compact crystal packing in which all F atoms of each anion engage in short C–H···F contacts. The 180 K phase transition of $(FA)_2X$ originates from the CDW instability of each FA stack, which has a half-filled band dispersive along the *a*-direction. The FA molecules within each stack are closely packed, so the expected dimerization of each FA stack should involve rotations of adjacent FA dimers around the stacking axis in opposite directions. It is probable that the formation of domain structures in each FA stack, introduced by rotational kinks, prevents the observation of a dimerized structure by single-crystal X-ray diffraction. The STM image observed for the (011) surface of $(FA)_2PF_6$ is explained if a few FA molecules under the tip apex undergo a rotational rearrangement around the stacking axis. Consideration of the short intermolecular H···H contact distances indicates that this rearrangement is a local phenomenon and is reversible.

## Acknowledgements

Work at North Carolina State University was supported by the Office of Basic Energy Sciences, Division of Materials Science, US Department of Energy. K.S.L.'s visit to North Carolina State University was supported by a grant from the Ministry of Education, South Korea.

## References

[1] Ch. Kröhnke, V. Enkelmann and G. Wegner, *Angew. Chem., Int. Ed. Engl., 19* (1980) 912.
[2] H. Eichele, M. Schwoerer, Ch. Kröhnke and G. Wegner, *Chem. Phys. Lett., 77* (1981) 311.
[3] V. Enkelmann, B.S. Morra, Ch. Kröhnke and G. Wegner, *Chem. Phys., 66* (1982) 303.
[4] W. Höptner, M. Mehring, J.U. von Schütz, H.C. Wolfe, B.S. Morra, V. Enkelmann and G. Wegner, *Chem. Phys., 73* (1982) 253.
[5] W. Stöcklein and G. Denninger, *Mol. Cryst. Liq. Cryst., 136* (1986) 335.
[6] Th. Schimmel, W. Riess, G. Denninger and M. Schwoerer, *Ber. Bunsenges. Phys. Chem., 91* (1987) 901.
[7] U. Köbler, G. Gmeiner and E. Dormann, *J. Magn. Magn. Mater., 69* (1987) 189.
[8] V. Enkelmann and K. Göckelmann, *Ber. Bunsenges. Phys. Chem., 91* (1987) 950.
[9] G. Sachs, E. Pöhlmann and E. Dormann, *J. Magn. Magn. Mater., 69* (1987) 131.
[10] M. Mehring, M. Helmle, D. Köngeter, G.G. Marcsch and S. Demuth, *Synth. Met., 19* (1987) 349.
[11] E. Dormann, *Synth. Met., 27* (1988) B529.
[12] Th. Schimmel, B. Koch, H.P. Geserich and M. Schwoerer, *Synth. Met., 33* (1989) 311.
[13] D. Köngeter and M. Mehring, *Phys. Rev. B, 39* (1989) 6361.
[14] V. Enkelmann, *Synth. Met., 41–43* (1991) 2547.
[15] W. Riess, W. Schmid, J. Gmeiner and M. Schwoerer, *Synth. Met., 41–43* (1991) 2261.
[16] W. Brütting, W. Riess and M. Schwoerer, *Ann. Phys., 1* (1992) 409.
[17] V. Ilakovac, S. Ravy, J.P. Pouget, W. Riess, W. Brütting and M. Schwoerer, *J. Phys. (Paris) IV, 3* (1993) 137.
[18] W. Riess and W. Brütting, *Phys. Scr., 49B* (1993) 721.
[19] K.F. Thier and M. Mehring, *Phys. Rev. B, 50* (1994) 2142.
[20] W. Brütting and W. Riess, *Acta Phys. Pol. A, 87* (1995) 785.
[21] W. Riess, W. Brütting and M. Schwoerer, *Synth. Met., 55–57* (1993) 2664.
[22] P.H. Nguyen, G. Paasch, W. Brütting and W. Riess, *Phys. Rev. B, 49* (1994) 5172.
[23] J.M. Williams, H.H. Wang, T.J. Emge, U. Geiser, M.A. Beno, K.D. Carlson, R.J. Thorn, A.J. Schultz and M.-H. Whangbo, *Prog. Inorg. Chem., 35* (1987) 51.
[24] M.-H. Whangbo, D. Jung, J. Ren, M. Evain, J.J. Novoa, F. Mota, S. Alvarez, J.M. Williams, M.A. Beno, A.M. Kini, H.H. Wang and J.R. Ferraro, in G. Saito and S. Kagoshima (eds.), *The Physics and Chemistry of Organic Superconductors*, Springer, Berlin, 1990, p. 262.
[25] M.-H. Whangbo and R. Hoffmann, *J. Am. Chem. Soc., 100* (1978) 6093.
[26] G. Bar, S.N. Magonov, H.-J. Cantow, J. Meiner and M. Schwörer, *Ultramicroscopy, 42–44* (1992) 644.
[27] J. Tersoff and D.R. Hamman, *Phys. Rev. B, 31* (1985) 805.
[28] S.N. Magonov and M.-H. Whangbo, *Adv. Mater., 6* (1994) 335.
[29] S.N. Magonov and M.-H. Whangbo, *Surface Analysis with STM and AFM*, VCH, Weinheim, 1995.
[30] J.J.P. Stewart, *QCPE Program No. 455.*
[31] A. Bondi, *J. Phys. Chem., 68* (1964) 441.
[32] This estimate was made from the following observations: the observed H···F distance of the N–H···F hydrogen bond is 0.10 Å shorter than the observed H···O distance of the N–H···O bond, and the observed H···O distance of the C–H···O distance is 2.30 Å: W.C. Hamilton and J.A. Ibers, *Hydrogen Bonding Solids*, Benjamin, Elmsford, NY, 1968, p. 16.
[33] H. Bengel, H.-J. Cantow, S.N. Magonov and M.-H. Whangbo, *Adv. Mater., 7* (1995) 5.
[34] H. Bengel, H.-J. Cantow, S.N. Magonov, D. Jung, J. Ren and M.-H. Whangbo, *New J. Chem.*, in press.
[35] H. Bengel, H.-J. Cantow, S.N. Magonov, H. Hillebrecht, G. Thiele, W. Liang and M.-H. Whangbo, *Surf. Sci.*, in press.
[36] W. Liang, M.-H. Whangbo, M. Evain, L. Moncoduit, R. Brec, H. Bengel, H.-J. Cantow and S.N. Magonov, *Chem. Mater., 6* (1994) 678.
[37] H. Bengel, H.-J. Cantow, S.N. Magonov, L. Monconduit, M. Evain and M.-H. Whangbo, *Surf. Sci. Lett., 321* (1994) L170.